Polarized rainbow

G. P. Können and J. H. de Boer

The Airy theory of the rainbow is extended to polarized light. For both polarization directions a simple analytic expression is obtained for the intensity distribution as a function of the scattering angle in terms of the Airy function and its derivative. This approach is valid at least down to droplet diameters of 0.3 mm in visible light. The degree of polarization of the rainbow is less than expected from geometrical optics; it increases with droplet size. For a droplet diameter >1 mm the locations of the supernumerary rainbows are equal for both polarization directions, but for a diameter <1 mm the supernumerary rainbows of the weaker polarization component are located between those in the strong component.

I. Introduction

Since the days of Airy[1] the theory of the rainbow is well established. In the beginning of the 19th century he showed that the wave front emerging from a water droplet is well approximated by a cubic law near the ray of minimum deviation (Descartes ray). The interference pattern of light from such a wave front was found to be given by a new function $Ai(z)$, which is oscillating for negative arguments and drops to zero for positive z. Later this function was called the Airy function after its discoverer. The intensity distribution of the rainbow is then proportional to $Ai^2(z)$, where $z \propto \theta_R - \theta$. Here θ denotes the scattering angle and θ_R the angle of minimum deviation, which is the rainbow angle in geometrical optics. This Airy solution is in good agreement with the observed features of the rainbow for droplet diameters larger than a few tenths of a millimeter. Even the exact solution of the rainbow problem (worked out with numerical methods) shows only minor deviations from Airy's results.[2]

There remains, however, a feature of the rainbow where Airy's description breaks down. As shown by Biot[3] in the beginning of the 19th century, rainbow light is strongly polarized, with the direction of the **E** vector tangential to the rainbow. The reason for this is that light rays, responsible for the rainbow, are always at least reflected once inside the water droplet; for the Descartes ray this reflection occurs close to the Brewster angle. Now it appears that the intensity distribution of the weaker (radial) polarized component of rainbow light differs completely from the Airy solution. In fact, where the strong component shows a maximum intensity (a supernumerary bow), the weaker one has a minimum. In other words, the supernumerary rainbows in the weaker component are shifted to the locations of the minima in the stronger component, a feature that was first experimentally observed by Bricard[4] for fog bows in 1940.

The reason for this shift is easy to understand.[5] Let us call the weaker component the polarized rainbow and the stronger (tangential) one the common rainbow. The main contribution to supernumerary bows is interference of two light rays with a different impact on the droplet and the same scattering angle (Fig. 1). For the polarized rainbow, the vibrations of light (**E** vector) are in the plane of incidence. If now the two angles of incidence are below and above the Brewster angle, respectively, an additional phase difference of 180° between the two interfering rays is introduced for the polarized rainbow; this does not occur for the common one (see Fig. 2). Therefore, interferences are destructive where they should be constructive without this phase jump. This results in a shift of the supernumerary bows for the polarized rainbow with respect to the common one. Numerical calculations of the polarized rainbow clearly show this behavior.[2] For the weaker secondary rainbow, formed after two internal reflections in the droplet, such a shift should be absent, since the phase jump of 180° is compensated by the second reflection. Nevertheless, for quantitative calculations Airy's formulas cannot be used in this case either, since one of his assumptions is that the amplitudes of the waves emerging from all parts of the cubic wave front are equal. For the polarized rainbow, however, there exists a sharp variation of the amplitude along the wave

G. P. Können is with Koninklijk Nederlands Meteorologisch Instituut, 3730 AE De Bilt, Postbus 201, The Netherlands, and J. H. de Boer is with Katholieke Universiteit, Mathematics Instituut, Nijmegen, The Netherlands.

Received 3 January 1979.
0003-6935/79/121961-05$00.50/0.

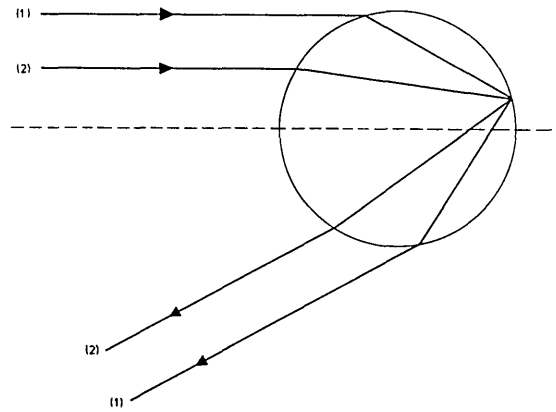

Fig. 1. Schematic diagram of the origin of supernumerary rainbows. Two light rays with a different impact on a rain drop may lead to scattering in the same direction. Interference between these rays arises from differences in their optical path lengths.

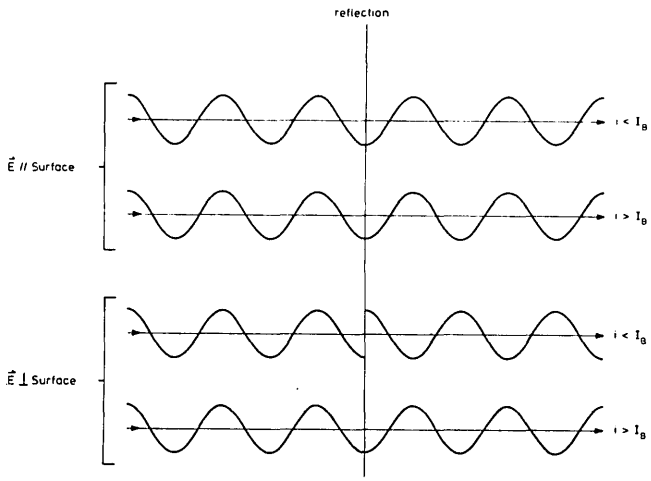

Fig. 2. Schematic view of the phase jump of a light wave by internal reflection inside a droplet for both polarization directions. I_B denotes the Brewster angle, i is the angle of incidence. Interference between two rays with $i < I_B$ and $i > I_B$ leads to a different interference pattern for the two polarization directions, due to the additional phase jump of 180° for $i < I_B$ in the lower part of the figure. Such interference plays an important role in rainbow formation. Apart from the phase jump illustrated here, a weakening of the waves occurs at reflection. This is not shown in the diagram.

front due to the variation of the Fresnel reflection coefficient near the Brewster angle.

As far as we know, a simple extension of Airy's rainbow theory to polarized light does not so far exist. In this paper we present an Airy solution for the polarized rainbow, obtained by incorporating the first-order variation of the Fresnel reflection coefficients into his formalism. This yields a simple expression for this intensity distribution in terms of the Airy function itself and its derivative. In the validity domain of Airy's theory, the resulting intensity distribution compares well with those obtained by numerical techniques from more sophisticated approaches.[2] From this analytic expression, general conclusions can be drawn about the intensity distribution of the polarized rainbow as a function of droplet size, as well as for the degree of polarization of rainbow light.

II. Calculation of the Rainbow Intensity Distribution

In this Section we primarily use Humphreys[6] notation. We first choose orthogonal coordinates x,y and take the origin at the point of inflection of the wave front emerging from the droplet. Let y be parallel to the Descartes ray. In the Airy approximation, this wave front can be represented by the curve

$$y = [h/(3a^2)]x^3, \tag{1}$$

where a is the radius of the droplet, and h is a constant with a value of 4.9 for the primary rainbow in water and 28 for the secondary rainbow.[6] This constant depends only weakly on the index of refraction n. Also, i and r are the angle of incidence and refraction at the droplet, I_B and R_B are these angles for Brewster reflection, where reflected light is completely polarized, and I_R is the angle of incidence for minimum deviation. We define $\alpha = i - I_R$ and $\theta_d = \theta - \theta_R$, i.e., the scattering angle minus the geometrical rainbow angle; $\theta_d = 0$ corresponds to scattering in the direction of minimum deviation. We have[6]

$$x = a\alpha \cos I_R. \tag{2}$$

The total vibration $V(t)$ of the waves in the direction θ_d is given by

$$V(t) = \int_{-\infty}^{\infty} k(x) \sin(\omega t - \delta) dx, \tag{3}$$

where $k(x)$ is the amplitude of the waves per unit of length of the front, and δ is the phase shift of a wave in direction θ_d from position x with respect to a wave from $x = 0$ in the same direction. Here ω is the angular frequency of the light concerned. Thus

$$\begin{aligned} V(t) &= \int_{-\infty}^{\infty} k(x) \cos\delta dx \sin\omega t - \int_{-\infty}^{\infty} k(x) \sin\delta dx \cos\omega t \\ &\equiv A \sin\omega t - B \cos\omega t. \end{aligned} \tag{4}$$

The intensity Int in a given direction is then

$$Int = A^2 + B^2. \tag{5}$$

For the cubic wave front we have, provided θ_d is not large,[6]

$$\delta = \frac{2\pi}{\lambda}\left(\frac{hx^3}{3a^2} - x\theta_d\right). \tag{6}$$

Hence

$$\left.\begin{aligned} A &= \int_{-\infty}^{\infty} k(x) \cos\frac{2\pi}{\lambda}\left(\frac{hx^3}{3a^2} - x\theta_d\right) dx, \\ B &= \int_{-\infty}^{\infty} k(x) \sin\frac{2\pi}{\lambda}\left(\frac{hx^3}{3a^2} - x\theta_d\right) dx \end{aligned}\right\}, \tag{7}$$

where λ is the wavelength of the light. Following Airy, we put $k(x) = 1$ for the common rainbow. In that case $B = 0$ since δ is antisymmetric in x, and we obtain the

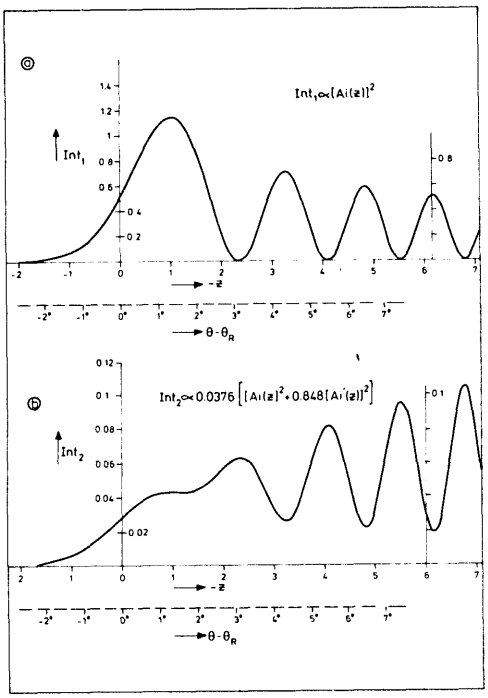

Fig. 3. The intensity distribution as a function of angle for the rainbow at both polarization directions, for $2\pi a = 1500\lambda$. This corresponds to a droplet radius of about 0.14 mm in visible light. The differences in locations of the supernumerary rainbows can be clearly seen from the graphs. Curve (a) represents the common rainbow, curve (b) the polarized rainbow, corresponding to the **E** vector tangential and radial with respect to the rainbow, respectively. The formulas used are given in the figure. The intensity scales are comparable. θ denotes the scattering angle; θ_R the rainbow angle.

Airy intensity distribution. For the polarized rainbow, however, $k(x)$ depends strongly on x. This dependence can be calculated from the reflection formulas of Fresnel. Since we are interested in the intensity distribution of the polarized rainbow with respect to the common rainbow we have to consider these formulas for both directions of polarization.

Let Am be the amplitude of a wave after one internal reflection and two refractions (as for the primary rainbow) and take the amplitude of the incoming wave as unity. We use the symbol Am_1 for light with the **E** vector perpendicular to the plane of incidence. Am_2 refers to light with this vector in the plane of incidence, as for the polarized rainbow. Then

$$\left.\begin{aligned} Am_1 &= -\left[1 - \frac{\sin^2(i-r)}{\sin^2(i+r)}\right]\frac{\sin(i-r)}{\sin(i+r)} \\ Am_2 &= \left[1 - \frac{\tan^2(i-r)}{\tan^2(i+r)}\right]\frac{\tan(i-r)}{\tan(i+r)} \end{aligned}\right\}. \tag{8}$$

Notice that Am_2 changes sign if $i + r$ passes 90 °, i.e., if i passes the Brewster angle I_B (Fig. 2).

For rainbow light the angle of incidence of the Descartes ray I_R is close to I_B, while $\tan I_B = n$. We define

$$\gamma = i - I_B, \qquad \epsilon = r - R_B. \tag{9}$$

According to Snell's law, $\sin i = n \sin r$ and $\cos i\,di = n \cos r\,dr$. Thus, for small γ,

$$\frac{1}{n}\frac{\cos I_B}{\cos R_B}\gamma = \epsilon; \qquad \epsilon = \frac{1}{n^2}\gamma = \frac{9}{16}\gamma \text{ for water } (n = 4/3). \tag{10}$$

Substituting γ and ϵ in Eq. (8) we have, for small γ,

$$Am_2/Am_1 \simeq (\gamma + \epsilon)/\cos^3(I_B - R_B), \tag{11}$$

where $\cos(I_B - R_B) = 0.96$ for water. Now we have $\alpha = i - I_R$ and $\gamma = i - I_B$ so that

$$\gamma = \alpha + I_R - I_B. \tag{12}$$

Since $k(x) = 1$ for the common rainbow we have from Eqs. (10), (11), and (12) for the polarized rainbow

$$\begin{aligned} k(x) = Am_2/Am_1 &= (\gamma + \epsilon)/\cos^3(I_B - R_B) \\ &= \frac{(1 + 1/n^2)\gamma}{\cos^3(I_B - R_B)} = 1.77\gamma \end{aligned}$$

for water. Remembering that $x = ax \cos I_R$ (2) this leads to

$$k(x) = \frac{1.77}{a \cos I_R}(x_0 + x), \tag{13}$$

with

$$x_0 = a(I_R - I_B)\cos I_R. \tag{14}$$

Substituting this in Eq. (7) and putting

$$-\frac{2\pi x \theta_d}{\lambda} \equiv uz, \quad \frac{2\pi h x^3}{3a^2\lambda} \equiv \tfrac{1}{3}u^3, \tag{15}$$

we find for the common rainbow the Airy expression[6]

$$\left.\begin{aligned} A &= 2\int_0^\infty \cos(\tfrac{1}{3}u^3 + zu)du\left(\frac{a^2\lambda}{2\pi h}\right)^{1/3} \\ &\equiv 2\pi\left(\frac{a^2\lambda}{2\pi h}\right)^{1/3} Ai(z) \\ B &= 0 \end{aligned}\right\}, \tag{16}$$

and for the polarized rainbow.

$$\left.\begin{aligned} A &= 2 \cdot \frac{1.77}{a \cos I_R} a \cos I_R (I_R - I_B)\int_0^\infty \cos(\tfrac{1}{3}u^3 + zu)du\,\frac{(a^2\lambda)^{1/3}}{2\pi h} \\ &= 2\pi \cdot 1.77(I_R - I_B)\left(\frac{a^2\lambda}{2\pi h}\right)^{1/3} Ai(z) \\ B &= 2 \cdot \frac{1.77}{a \cos I_R}\int_0^\infty u \sin(\tfrac{1}{3}u^3 + zu)du\left(\frac{a^2\lambda}{2\pi h}\right)^{2/3} \\ &= -2\pi\frac{1.77}{a \cos I_R}\left(\frac{a^2\lambda}{2\pi h}\right)^{2/3} Ai'(z) \end{aligned}\right\}, \tag{17}$$

with

$$z = -\left(\frac{4\pi^2 a^2}{h\lambda^2}\right)^{1/3}\theta_d. \tag{18}$$

If we postulate the intensity distribution for the common rainbow to be (arbitrary units)

$$Int_1 = [Ai(z)]^2, \tag{19}$$

then, according to Eq. (5), the polarized rainbow has the intensity distribution

$$Int_2 = [1.77(I_R - I_B)Ai(z)]^2 + \left(\frac{a^2\lambda}{2\pi h}\right)^{2/3}\left[\frac{1.77}{a \cos I_R}Ai'(z)\right]^2, \tag{20}$$

which is the final expression for the intensity distribution of the primary rainbow in both polarization directions. For water ($n = 4/3$) and visible light ($\lambda = 0.6\ \mu$m) this reduces further, expressing the droplet size in mm, to

$$\left.\begin{aligned} Int_1 &= [Ai(z)]^2 \\ Int_2 &= 0.0376[Ai^2(z)] + 0.232a^{-2/3}[Ai'(z)]^2 \end{aligned}\right\}, \tag{21}$$

where $z = -4.92a^{2/3}\theta_d$ if θ_d is expressed in degrees.

III. Applications

A. Supernumerary Rainbows

Figure 3 represents the intensity distribution for both polarization directions of a rainbow with $n = 4/3$ and $2\pi a = 1500\lambda$, corresponding to a droplet radius a of $\sim$0.14 mm in visible light ($\lambda = 0.6\ \mu$m). The same situation has been calculated numerically,[2] using the complex angular momentum theory, yielding almost the same curve. Apparently, not only the Airy theory itself,[2,5] but also our extension can be applied at least down to such small droplet radii. Figure 3 shows clearly the differences in locations of the maxima for both polarization directions. This shift remains present for much smaller droplet sizes,[4,2] where Airy's theory gives qualitative information only.[5]

From our formulas, it is easy to calculate the upper limit of the droplet radius where the maxima and minima are interchanged for the two polarization directions. For this, we use

$$\left.\begin{aligned} Ai(-z) &\simeq \pi^{-1/2}z^{-1/4}\cos(\tfrac{2}{3}z^{3/2} - \pi/4) \\ Ai'(-z) &\simeq \pi^{-1/2}z^{1/4}\sin(\tfrac{2}{3}z^{3/2} - \pi/4) \end{aligned}\right\} \tag{22}$$

These approximations already hold well for $z > 2$. Notice that $Ai^2(-z)$ is zero where $Ai'^2(-z)$ shows a maximum and vice versa. Substituting (22) in (21), we have for the oscillating part of the intensity distribution for the polarized rainbow

$$Int_2 = 0.0376\pi^{-1}z^{-1/2}[1 + (0.232a^{-2/3}z - 1)\sin^2(\tfrac{2}{3}z^{3/2} - \pi/4)]. \tag{23}$$

Thus, if

$$0.232a^{-2/3}z - 1 > 0, \tag{24}$$

the oscillations of the polarized rainbow are in phase with those of $Ai'^2(z)$ and thus out of phase with those of the common rainbow. Taking $z \cong 3$ as a representative value (Fig. 3), this means that for $a > 0.6$ mm the oscillations in the intensity distribution for both rainbows are in phase and for $a < 0.6$ mm out of phase. If we further assume the oscillating character of the polarized rainbow to be only visible if its intensity at a maximum is at least twice that of an adjacent minimum, we find $a > 1.7$ mm and $a < 0.2$ mm, respectively.

From Sec. II it is clear that the droplet radius below which the oscillations are out of phase depends strongly on $I_R - I_B$, i.e., on the index of refraction n. The most extreme case is for $I_R = I_B$, i.e., if the Descartes ray reflects at the Brewster angle. This is the case for $n = \sqrt{2}$ (Ref. 7). Then, the intensity distribution of the polarized rainbow is only proportional to $a^{-2/3}Ai'(z)^2$ and maintains its out of phase character for any droplet size. For water, n is so close to $\sqrt{2}$ that this behavior is already present for a relatively large droplet radius.

The formalism of Sec. II is also applicable to the common rainbow, if one wishes to introduce the variation of the reflection coefficient with i. This is lacking in the Airy theory itself. Then for the common rainbow one obtains also an intensity distribution $Int_1 \propto Ai^2(z) + CAi'^2(z)$, but here the constant C is small. Therefore $Ai'(z)$ never becomes the leading function in this expression and represents only a small correction to the original Airy formula. This second term, however, causes the minima to be nonzero, in agreement with the findings of numerical calculations.[2] Finally, the weaker secondary rainbow (formed after two internal reflections in the drop) can be calculated along the same lines that we did for the primary rainbow. However, here $I_R - I_B$ is much larger, so that deviations from the Airy formulas are less pronounced, even for the polarized rainbow.

For the secondary polarized rainbow, the main characteristics are given by $Int_2 \propto Ai^2(z) + CAi''^2(z)$; for $n = \sqrt{3}$ (reflection of the Descartes ray at the Brewster angle) only $Int_2 \propto Ai''^2(z)$ remains. However, since $Ai''(z) = zAi(z)$, the oscillations of the polarized rainbow remain always in phase with those of the common rainbow, which follows also from the simple argument[5] mentioned in Sec. I.

B. Degree of Polarization

In geometrical optics, the ratio $R = Int_2/Int_1$ can be easily calculated for the Descartes ray, yielding $R = 0.039$ for the primary rainbow.[7] Putting $z = 0$, we find for rainbow scattering in the angle of minimum deviation from Eq. (21)

$$R = 0.0376 + 0.00465a^{-2/3}, \tag{25}$$

which gives $R = 0.0376$ for $a \to \infty$. This is close to 0.039. However, R increases with decreasing a and is already 0.054 for $a = 0.14$ mm. Apparently, if I_R is close to I_B, geometrical optics cannot be used for calculations of R (see Ref. 7), since in that case the contributions from other parts of the wave front to scattering at $\theta_d = 0$ cannot be neglected, always causing a higher value of R.

For small a, it makes sense to consider the ratio R of the maxima in the intensity distributions rather than for $\theta_d = 0$. Taking for the common rainbow $z = -3.25$ and for the polarized one $z = -4.08$ as representative maxima (both can be considered as a first supernumerary bow), we find from Eq. (21) that

$$R = 0.0087a^{-2/3}[Ai'(-4.08)/Ai(-3.25)]^2 = 0.032a^{-2/3}, \tag{26}$$

which has even a value of 0.12 for $a = 0.14$ mm. For such small droplets, the polarized rainbow is thus much easier to observe than one would infer from geometrical optics. Although our formalism gives for fog qualitative information only, in this case[2] the polarized rainbow and the shift of its supernumerary bows can be expected to be visible in nature.

IV. Conclusion

In this paper it has been shown that the intensity distribution function of the rainbow for both polarization directions can be obtained from Airy's equations, if the variation of the amplitude of light along the wave front is taken into account.

This yields a simple analytic expression for the intensity distribution of light near the rainbow angle, which compares well with results obtained by more complicated theories. For the primary rainbow the locations of the supernumerary maxima and minima are interchanged for both polarization directions; an upper limit of the droplet size is calculated where this behavior remains present. The degree of polarization of the rainbow is less than expected from simple geometrical optics, indicating that the out of phase character of the supernumerary rainbows for both polarization directions will be visible in nature, probably at best for fog bows.

References

1. G. B. Airy, see any textbook on meteorological optics.
2. V. Khare and H. M. Nussenzveig, Phys. Rev. Lett. **33**, 976 (1974); H. M. Nussenzveig, Sci. Am. 16 (April 1977).
3. C. Boyer, *The Rainbow, from Myth to Mathematics* Yoseloff, New York, 1959).
4. J. Bricard, Ann. Phys. 14, 148 (1940).
5. H. C. van de Hulst, *Light-Scattering by Small Particles* (Wiley, New York, 1957), pp. 249 *et seq.*
6. W. J. Humphreys, *Physics of the Air* (McGraw-Hill, New York, 1940), pp. 476 *et seq.*
7. S. Rösch, Appl. Opt. **7**, 233 (1968).

Books *continued from page 1960*

article by **P. E. Anuta,** who also discusses the application of fast Fourier transform (FFT) techniques to cross-correlation in order to determine spatial distances. This author also presents a method of achieving translational, rotational, and scaling corrections between images. However, cross-correlation requires the use of normalized correlation surfaces, and the FFT method can only be applied to the nonnormalized part. The memory requirement of this technique may also render it infeasible for large search areas (size larger than 256 × 256 pixels). Procedures other than correlation are considered in the next two articles, respectively by **D. I. Barnea** and **H. F. Silverman,** and by **W. F. Webber,** the so-called *sequential similarity detection algorithms* (SSDA). Indeed, aside from tradition and expediency, there is no justification for using correlation to solve all digital registration problems. Algorithms that have selectable distance measure properties and lower computational complexity are proposed and illustrated in the case of translational imagery. An affine transformation is discussed and illustrated by **R. A. Emmert** and **C. D. McGillem.** Alternatively, **W. K. Pratt** proposes a linear spatial preprocessing of the images to be registered by utilizing the spatial correlation with each image prior to the application of a correlation measure. This is accomplished by extending the correlation measure to include the statistical properties of each of the images being registered. This technique appears to provide a considerable improvement in the detectability of image misregistration. **C. D. McGillem** and **M. Svedlow** propose using concepts derived from statistical estimation theory. Specifically, the error variance in the registration of two different images of the same scene is suggested as a measure of the overlay quality in a manner analogous to that employed in a radar system during error determination of the measured delay time. Two different models based on quite different assumptions are proposed and applied to Landsat I; both were found to yield a variance that is a function of the effective bandwidth of the signal and the noise, and the signal-to-noise ratio.

Image Enhancement for Manual Interpretation is the subject of Part 4, organized by **P. Anuta.** Technology applicable to the manual extraction of information from an image is here addressed. Improvements in this area have resulted from a better understanding of the human visual response mechanism, restoration and improvement of the data quality, and data enhancement for visual perception for separating information from background. Early developments in the Jet Propulsion Laboratory's Image Processing Laboratory are briefly reviewed by **D. A. O'Handley** and **W. B. Green.** These include removal of geometric distortion and residual image effects, and applications to biomedicine, forensic sciences, and astronomy. **M. M. Sondhi** reviews the digital restoration techniques from the point of view of space-domain and spatial frequency domain descriptions of images. These include inverse filtering, minimization of mean-squared errors, and constrained deconvolution. Image restoration, mathematically speaking, amounts to the solution of first-kind Fredholm integral equations for which a large body of literature now exists. Hence, a wealth of techniques may be available for application to this particular problem. Digital image processing, in general, is excellently reviewed by **B. R. Hunt,** who concentrates upon image formation and recording processing, digital sampling and image display, and image coding and restoration. Restorations by use of an eye-model constraint and nonlinear restoration by maximization of the posterior density function are also proposed. The structure of images and its compatibility with the processes used to store, transmit, and modify them is the subject of a highly interesting exposition by **T. G. Stockham, Jr.,** who also emphasizes the harmony of density representation and multiplicative processing with the physics of image formation. These and other observations are used to present a visual model which is subsequently used for providing an objective criterion for image quality based upon that model.

The natural extension of the topic of Part 4, namely, information extraction by computers as opposed to human operators, is addressed in Part 5, organized by **P. E. Anuta** and **A. Rosenfeld.** The introductory article by **R. L. Lillestrand** dwells on techniques for the detection of changes in images of the same scene by presenting to the human observer only the changes, as opposed to all the information contained in the images. To reduce noise in the difference picture to acceptably low levels, spatial alignment of the various parts of the image must be highly accurate. The corresponding requirements are detailed in the contribution. In an excellent article, **G. Nagy** surveys the experimental developments in digital image processing prompted by major national environmental remote-sensing programs. Importantly, it also attempts to identify the value and promise of the several aspects of current research lines in the field and to assess the contribution to be expected from them. This is a welcome sobering note with a plea for the better exploitation of talents and funds committed to this endeavor. **F. C. Billingsley** reviews the digital image processing developed at JPL and discusses briefly the multispectral processing developed at the Laboratory for the Application of Remote Sensing of Purdue University. These include geometrical stretching, vignetting removal, enhancement of high spatial frequency content, etc., which are abundantly illustrated utilizing spacecraft images. These techniques are shown to have been successfully applied to images from a variety of sources (biomedical, forensic, time-lapse photography, etc.), and dramatically illustrated in these several instances. Applications of pattern recognition techniques to remote sensing of the earth's atmosphere are subsequently reviewed by **K.-S. Fu.** The several recognition techniques can be conveniently classified in two groups: decision-theoretic (or statistical) and syntactic (or structural or linguistic). However, as suggested later in this volume by **L. Kanal,** too much stress on this distinction hides many simi-

continued on page 1987